

Understanding soil loss in mollisol permanent gully head cuts by hydrological and hydromechanical-mechanical response

Chao Ma¹, Shoupeng Wang¹, Dongshuo Zheng¹, Yan Zhang¹, Jie Tang², Yanru Wen³, Jie Dong⁴

¹ School of Soil and Water Conservation, Beijing Forestry University, Beijing 100083, PR China-

² Advanced Institute of Natural Sciences, Beijing Normal University at Zhuhai, Zhuhai 519087, China

³ Institute of Agricultural Resources and Regional Planning, Chinese Academy of Agricultural Sciences, Beijing 100081, China

⁴ Civil and Environmental Engineering Department, Clarkson University, NY, 13699, USA-

Corresponding Author: Professor Chao Ma, sanguoxumei@163.com

Abstract: During permanent gully development, soil losses on steep slopes and in channel beds are typically driven by the hydromechanical response and water storage within the soil mass, ~~while; however, such this~~ knowledge ~~have~~ ~~has~~ been largely neglected in previous studies of gully erosion in the mollisol region of Northeast China. In this study, erosion intensities during the 111 d of the rainy season and 97 d of the snow-melting season were analyzed with respect to soil water storage ~~and~~ drainage capacity, ~~and~~ soil suction stress, supported by ~~the~~ monitoring results of soil moisture, temperature, and precipitation, ~~as well as~~ ~~and~~ experimental analysis of soil hydromechanical properties. Under the same confining stress, the mollisols in the interrupted head cut of Gully No. II increased more rapidly and dissipated pore water pressure more ~~than effectively than those~~ at the uninterrupted head cut of Gully No. I. The combination of the soil water characteristic curve and the hydraulic conductivity function ~~indicates~~ ~~indicated~~ that the mollisols of Gully No. II had a lower air-entry pressure and higher saturated hydraulic conductivity during the wetting and drying cycles than Gully No. I. The head cut area of Gully No. II exhibited rapid ~~response of~~ water infiltration and drainage; ~~response~~ and high soil water storage capacity. The absolute suction stresses within the mollisols of Gully No. II was lower than that in Gully No. I, which could lead to high erosion per unit of steep slope area. Importantly, gravitational mass wasting on steep slopes ~~is was~~ closely related to soil suction stress, and we observed a correlation between erosion per unit ~~in the~~ gully bed area and ~~the~~ soil water storage. Therefore, it is more important to predict the soil loss in ~~the~~ permanent gully from ~~both~~ soil water storage and the hydromechanical response of soil mass, other than sole rainfall amount. In other words, the required water storage capacity to ~~produce~~ ~~yield~~ runoff intensity and low suction stress would ~~give more accurate results in predicting~~ soil loss in the permanent gully head-cut ~~more accurately~~.

Keywords: Gravitational mass wasting; Soil water characteristic curve; Erosion per unit area

1 Introduction

Gravitational mass wasting refers to the downward movement of rock, regolith, and/or soil caused by gravity along the sloping top layers of the earth's surface (Evans, 2004; Allen et al., 2018). There are four types of mass wasting, based on the speed of movement of the material and the level of moisture, namely, falls and avalanches, landslides, flow, and creep (Bierman and Montgomery, 2014). They often occur in various sizes with undetermined failure planes and are affected by hydrological and hydromechanical responses (Stein and LaTray, 2002; Rengers and Tucker, 2014). On the steep slopes of permanent gullies, gravitational mass wasting involves debris-free soil falling owing to bed undercutting driven by intensive channelized flow or persistent high soil moisture (Harmon and

43 Doe, 2001). Soil loss from gravitational mass wasting during the rainy season occurs when a steep slope loses support
44 from debris deposits. Meanwhile, soil loss during the melting season may result from persistent low soil suction
45 stress. In unsaturated soil mechanics, a high occurrence potential or intensive soil loss from gravitational mass
46 wasting corresponds to low soil suction stress (Lu and Godt, 2013). It remains unclear whether soil loss from
47 gravitational mass wasting corresponds to soil suction stress during these two stages.

48 Permanent gullies are initiated in locations where concentrated flows can erode and deliver bed sediments
49 (Kirkby and Bracken, 2009; Sidle et al., 2017) and expand when gravitational mass wasting occurs following instant
50 or constant water infiltration (Poesen et al., 2010; Tebebu et al., 2010). Permanent gully development can be
51 determined by the topographical threshold and volumetric retreat rate of gully head cuts (Svoray et al., 2012; Guan
52 et al., 2021; Zare et al., 2022), the gully length–area–volume relationship (Li et al., 2015 and 2017), and their function
53 in the upstream drainage area and rainy days in different environments (Hayas et al., 2019). Soil loss from permanent
54 gullies is largely influenced by hydrological factors (Gómez-Gutiérrez et al., 2012), such as the flow rate, total water
55 volume, rainfall intensity and amount, and hydromechanical properties of the soil mass. Soil properties are affected
56 by land use, plant roots, texture, and structure. The hydrological process near the head cut, the hydromechanical
57 response of soil mass in reaction to water infiltration, and their relationship with soil loss from gravitational mass
58 wasting remain unknown. Under natural conditions, water infiltrates either following rain events or snow/ice-
59 melting events. The infiltration rate strongly depends on ~~both~~ the amount and intensity of precipitation, ~~which~~
60 ~~lead~~sing to soil water storage. However, the amount of stored water varies ~~owing due~~ to the amount of rainfall and
61 ~~the~~ melting rate or temperature. During the snow/ice-melting season, ~~the the duration of~~ water infiltration duration
62 persists longer than ~~that of~~ rain events because of prolonged soil saturation and an extended period of low soil suction
63 stress. This may generate more soil loss owing to gravitational mass wasting. However, rain events typically generate
64 intensive channelized flows, which erode steep slopes and trigger gravitational mass wasting. Therefore, it is
65 challenging to compare soil loss in the two seasons. However, this issue could be addressed by considering the
66 associated hydrological processes of head cuts and hydromechanical responses within the soil mass.

67 In the mollisol region of Northeast China (MEC), over 296,000 permanent gullies have developed since 1960
68 (Yang et al., 2017; Dong et al., 2019). Gravitational mass-wasting processes have caused rapid gully widening due
69 to overfarming and a lack of maintenance (Wang et al., 2009). Various studies have focused on the hydrological
70 processes affecting ephemeral gully development and volume disparities caused by rain/snow melting (Tang et al.,
71 2022; Jiao et al., 2023), tillage practices (Xu et al., 2018; Li et al., 2021), and morphology (Zhang et al., 2016).
72 Permanent gullies pose a greater threat to croplands than ephemeral gullies because the soil loss from permanent
73 gully erosion can be as high as 50–65% of the total loss (Zhang et al., 2022). The relatively high ~~area-area~~-increasing
74 ratio is affected by the combination of permanent gullies with cropland use, a large ridge orientation angle, and a
75 sunny orientation (Li et al., 2016; Liu et al., 2023). Tang et al. (2023) provided evidence of the rainfall threshold for
76 permanent gully development ~~and~~. They found that the maximum value of 3-d ~~aca~~ cumulative rainfall best explained
77 permanent gully bed erosion, and the cumulative value of erosive rainfall best accounted for gravitational mass
78 wasting. However, gravitational mass wasting on the steep slope of a permanent gully can occur either during the
79 rainy season or snow-~~melting~~ season (Zhang et al., 2020; Zhou et al., 2023). Note that some studies proved that the
80 soil loss during snow-melting season remarkably accounts for a large percentage (Hu et al., 2007 and 2009), and
81 gully heads retreated faster than in the summer (Wu et al., 2008). Currently, the hydrological processes near the head
82 cut and the hydromechanical response of mollisols to water infiltration in the two seasons have never been
83 documented, and the associated soil loss from gravitational mass wasting is poorly understood. In the MEC, although
84 the duration of the snow/ice-~~melting~~ season is shorter than that of the accumulated rainy days (Wang et al., 2021;
85 Fan et al., 2023; Went et al., 2024), the time for snow-~~melting~~ water ~~is far more than~~ significantly exceeds that of
86 rainy water infiltration. Therefore, soil water storage may ~~exceed surpass~~ drainage ~~because of~~ owing to continuous

87 meltwater infiltration and limited water drainage paths. Rain infiltration during the summer season temporarily
88 increases and then decreases once the rain event ceases and the water drains. Stored water significantly depends on
89 rainfall events and the initial soil water storage (Farkas et al., 2005; Xu et al., 2018). Therefore, the duration of low
90 soil suction stress, such as high soil moisture, differed substantially between the two seasons. Another effect is
91 channelized water during intensive rainstorms (Wen et al., 2021), which may erode the bed and result in gravitational
92 mass wasting. Therefore, the soil loss from gravitational mass wasting may coincide with the soil suction stress in
93 the snow/ice-melting season. Meanwhile, this coincidence may not exist in the rainy season.

94 Soil loss from gravitational mass wasting on the steep slope of a permanent gully is poorly understood in the
95 MEC. To date, relatively few studies have addressed its relationship with the hydrological and hydro~~mechanical-~~
96 ~~mechanical~~ response of the soil mass. This work ~~has~~ focused on how the monitored soil water change and the suction
97 stress affect soil loss during the rainy and melting seasons in the head cuts of two permanent gullies, where one head
98 cut experiences no human activity, whereas the other does. Soil loss in the head cut area during the rainy and melting
99 seasons was observed. The differences in the physical properties of the mollisols, such as pore water pressure
100 dissipation at a given confining stress, the soil water characteristic curve (SWCC), and the hydraulic conductivity
101 function (HCF), were compared. The soil loss per unit area on the steep slope and gully bed was analyzed for the
102 soil water storage, ~~drainage~~~~rainage~~, and ~~the~~ soil suction stress, respectively. The objective of this study ~~mainly~~
103 ~~exhibits~~~~was to characterize~~ the relationship between soil loss intensity on steep slopes and ~~the~~ hydro~~mechanical-~~
104 ~~mechanical~~ response of the soil mass, ~~and as well as~~ the intensity in channel beds with water storage.-

105 2 Study area

106 Northeast China is one of the three main mollisol regions worldwide, with a total area of 1,030,000 km². It
107 contributes 20% of the grain and more than 40% of the corn in China. Most of the mollisol region was gradually
108 converted from native vegetation to cropland beginning in the late 19th Century. Croplands constitute 80% of the
109 total land area, and the main crop types are soybean and corn. The study area is located in the typical heavy gully
110 erosion area of the mollisol region of Northeast China, where native grasslands and forests have been fully converted
111 into croplands since 1968. It is situated in a transitional rolling hilly area extending from the Songnen Plain to the
112 Greater Khingan Mountains in the west, the Lesser Khingan Mountains in the north, and near the Nen River (Fig.
113 1a). Owing to the gentle landscape, the farmland in the study area is covered by a thick black organic soil layer, with
114 sandstone, mudstone, and sandy conglomerate underneath.

115 The two permanent gullies examined in this work are 1.4 km apart and are located on the south-facing and
116 north-facing rolling slopes, respectively (Figs. 1b and 1c). The catchment area above Gully No. I is 0.22 km². The
117 relative relief and channel gradient are 25.85 m and 3.3%, respectively. The catchment above the head cut of Gully
118 No. II is 0.35 km², and the relative relief and channel gradient are 26.1 m and 3.2%, respectively. The width of Gully
119 No. I gradually broadened, whereas Gully No. II narrowed and Gully No. I was deeper (Figs. 2a and 2b). The mean
120 depth of the Gully No. I was 3.5 m while that of Gully No. II was 1.23 m. The mean length and width of No. I gully
121 were 25.3 m and 8.72 m, whereas those of Gully No. II were 28.2 and 5.61 m. The gully area for No. I was 199.3
122 m², and the volume was 863.6 m³. For Gully No. I, the area and volume of the gully were 143.3 m² and 123.6 m³.

123 The two gullies are still expanding because they are connected to the river network, which drains water into the
124 Nen River. Although grass covers the area near the sidewall and ridge along the gully, mass-wasting movement
125 frequently occurs during the melting and rainy seasons. The differences in the gully planform and depth indicate that
126 the mass movement at the sidewall or head cut has distinctive rates and scales. The mass movement at the sidewalls
127 of the two gullies differed in scale, as shown in Figs. 2c and 2d. The height and width of the Gully No. II were lower
128 than those of the Gully No. I (Fig. 3). The head cut area of Gully No. II underwent tillage activities, whereas the

head cut area of Gully No. I has did not. Therefore, Gully No. II is representative of the initial development stage for a large permanent gully.

The study area has a continental monsoon climate with variable annual precipitation ranging from 347 to 775 mm, with an average of 546 mm between 1971 and 2018 (Tang et al., 2023). Rainfall mainly occurs between June and August, accounting for 70–90% of the annual precipitation, with an average of 461 mm. Snowfall occurs mainly from November to April, accounting for 10–30% of the annual precipitation. The average temperature in the coldest and warmest months are $-22.5\text{ }^{\circ}\text{C}$ and $20.8\text{ }^{\circ}\text{C}$, respectively, with an annual average temperature of $0\text{ }^{\circ}\text{C}$.

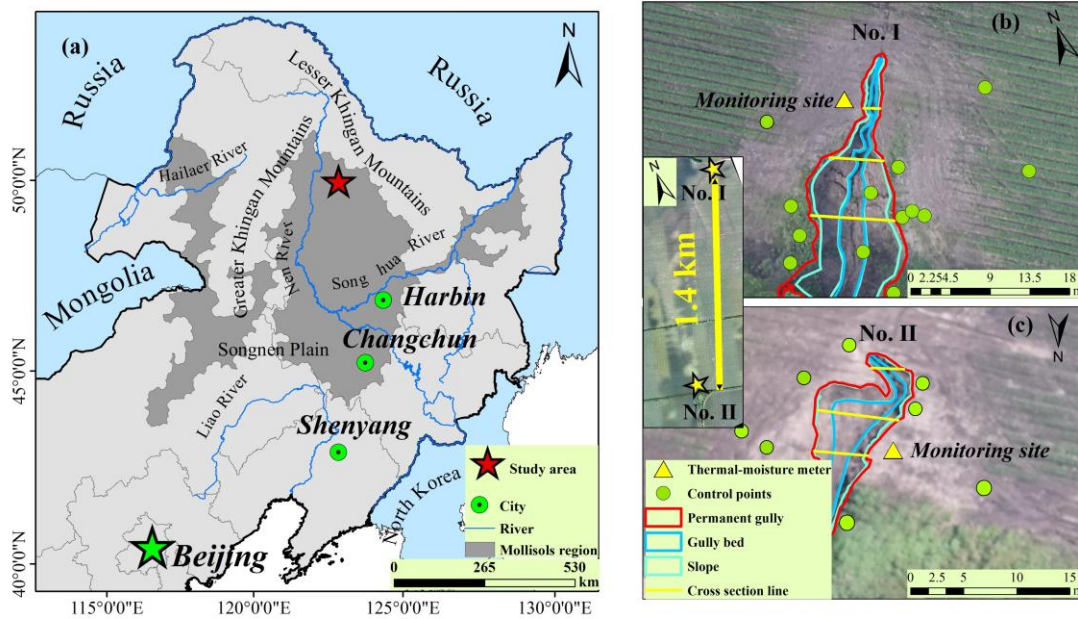
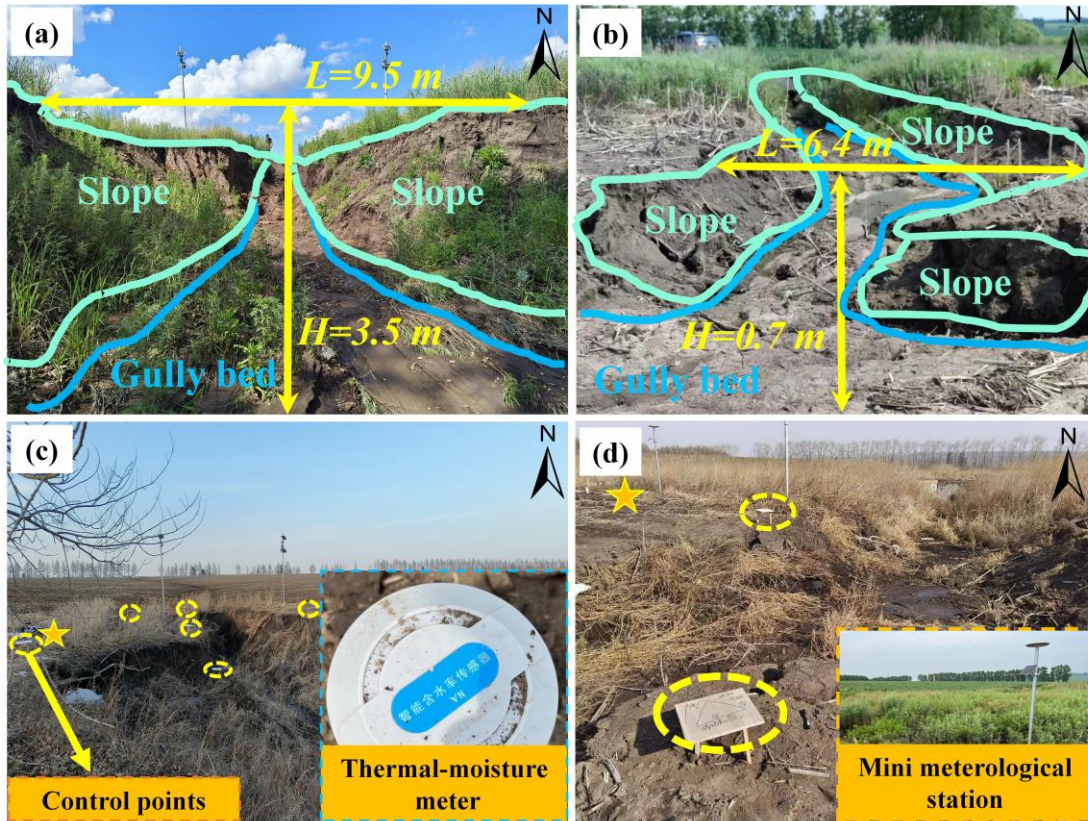
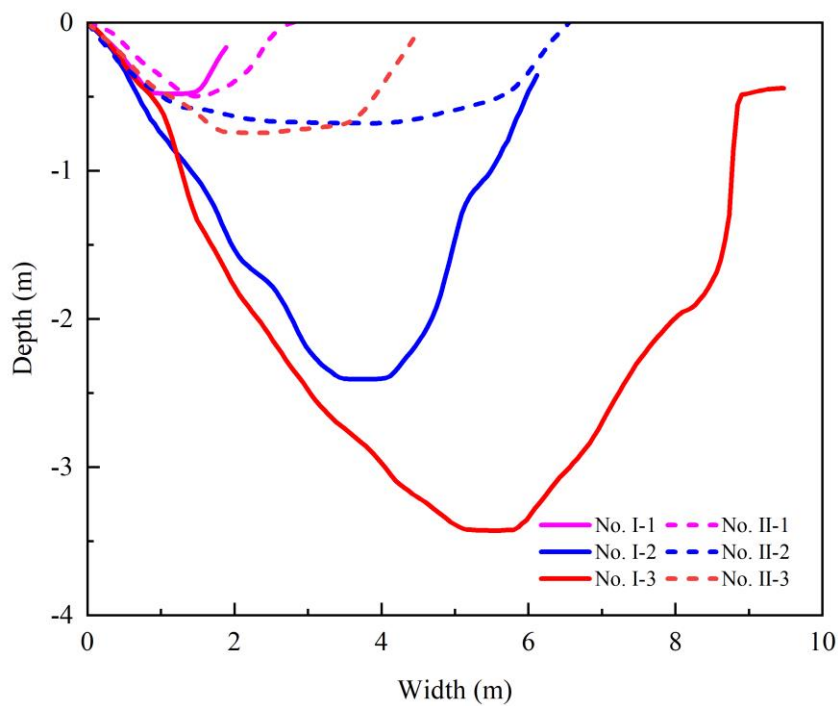


Fig. 1. Location of the two permanent gullies in the mollisol region of Northeast China. (a) The red star marks the observation site in the study area (from ESRI). (b) Monitoring sites and ground controlling points at permanent Gully No. I. (c) Monitoring sites and ground controlling points at permanent Gully No. II. (background of a is from ESRI. The area between the blue lines marks the gully bed, and the area that between the pink and blue lines marks the steep slope.



142
143
144
145
146
147
148

Fig. 2. A close view of the steep slope and head cut of the two permanent gullies, with (a) cross-section and upstream view of the permanent Gully No. I, (b) cross-section and downstream view of the permanent Gully No. II, (c) ground control points (blue dot circles) and the soil moisture–temperature monitoring site (yellow star) at permanent Gully No. I, and (d) ground controlling points and the soil moisture–temperature monitoring sites at permanent Gully No. II. The location of the head cut of the two gullies is shown in Fig. 1. The area between the blue lines marks the gully bed. The area between the pink and blue lines marks the slope.



149

150 **Fig. 3.** Difference of the two permanent gullies' cross-section. The location of the cross-section lines is shown in
 151 Figs. 1b and 1c.

152 **3 Material and methods**

153 **3.1 Monitoring work**

154 Near the gully head cut, frequency-domain reflectometry sensors were installed to monitor the soil moisture
 155 and air temperature at depths of 20, 40, 60, and 80 cm (Fig. 2c). These two monitoring sites share the same rainfall
 156 records as Gully No. II (Fig. 2d). A trench was dug to obtain soil samples from the two monitoring sites. The soil
 157 samples were used for pore water pressure dissipation tests via consolidated undrained triaxial compression tests
 158 (CU) using a GDS triaxial apparatus (GDS, UK), and the unsaturated permeability was measured using the transient
 159 release and imbibition method (TRIM; Lu and Godt, 2013).

160 To observe the gravitational mass-wasting process during the rainy and melting seasons, the study area was
 161 scanned using numerous control points (the dots in Figs. 1a and 1b and dashed circles in Figs. 2c and 2d) installed
 162 in and around the gully area, and an unmanned aerial vehicle (UAV) was used. These control points were used to
 163 improve the accuracy of the UAV-derived map and digital elevation model to obtain highly accurate topography
 164 data. Three flights on June 28, 2022, October 17, 2022, and June 20, 2023, were performed with the same flight
 165 routine and image overlap. The two frontier flights in 2022 spanned 111 d during the rainy season. The latter two
 166 covered the winter of 2022 and the spring of 2023. As low soil moisture persists from October each year and snow
 167 cover in the winter ~~season~~ does not result in gravitational mass movement, the effective duration of the melting
 168 season starts on March 15, 2023. Therefore, the melting season in this study lasted 97 d. We used Pix4D software to
 169 process the image synthesis and gully topography production, which can reallocate the point cloud and filter the
 170 points of the vegetation layer. As the points of the vegetation layer, mainly the grass blades, are changeable in plant
 171 height, whereas the ground point is fixable, the vegetation layer can be filtered out and removed using the filtering
 172 tool. The DEM products were spatially registered in ArcGIS 10.2 using a standard layer of orthoimages, ground
 173 control points, and spline functions (Table 1). The erosion depth of the head cut was then obtained from the
 174 difference between the two DEMs. Therefore, the linearity and erosion per unit area could be calculated using the
 175 erosion depth and grid size. The differences between the two digital elevation models generated positive and negative
 176 terrain, which showed soil loss from gravitational mass wasting. The eroded soil volume in a unit of steep slope
 177 surface area, termed erosion per unit area, was applied to address the erosion caused by gravitational mass wasting.

178
 179 **Table 1.** Detailed information of on three UAV flights and the digital elevation models

UAV model	Flight date	Season/ duration	Flight_ height (m)	DEM accuracy (m)	Image overlap (%)
DJI Inspire 2 RTK	2022.06.28	/	200	0.058	80
DJI Phantom 4 RTK	2022.10.17	Rainy/111 d	500	0.108	80
DJI Phantom 4 RTK	2023.06.21	Melting/97 d	150	0.042	80

180 181 **3.2 Tests of pore water pressure rising and dissipation**

182 The consolidation module of the GDS triaxial apparatus was used to record the pore water pressure within the
 183 soil mass under a given confining stress. The soil samples were initially saturated in a vacuum pump and then
 184 consolidated in the chamber of the GDS apparatus at effective confining pressures of 100, 200, and 300 kPa with a

185 10-kPa backpressure. The consolidation process was completed when the pore water pressure decreased to the
 186 backpressure values.

187 For the pore water increasing stage:

$$188 P_{\uparrow} = P_0 \times t^{b_{\uparrow}} \quad (1)$$

189 where P_{\uparrow} is the recorded pore water pressure during the increasing stage (kPa), P_0 is the initial pore water pressure
 190 since loading (kPa), t is the time (s), b_{\uparrow} is the rising proxy reflecting the steepness of the power-law curves of pore
 191 water pressure increase.

192 For the pore water dissipation stage:

$$193 P_{\downarrow} = \frac{P_{max}}{1+b_{\downarrow} \times t} \quad (2)$$

194 where P_{\downarrow} is the recorded pore water pressure during the dissipation stage (kPa), P_{max} is the maximal pore water
 195 pressure since loading (kPa) and is the rollover point in the pore water pressure curve, t is the time (s), b_{\downarrow} is the
 196 dissipation proxy reflecting the water drainage ability of soil mass at given confining pressure ~~and~~. It reflects the
 197 concavity of the pore water pressure dissipation curve.

198

199 3.3 Hydromechanical properties

200 TRIM was used to test the unsaturated permeability of the soil mass (Lu and Godt, 2013). The SWCC and HCF
 201 were obtained using Hydrus 1-D (Wayllace and Lu, 2012). Using the models proposed by Mualem (1976) and van
 202 Genuchten (1980), the constitutive relations between the suction head (h), water content (θ), and hydraulic
 203 conductivity (K) under drying and wetting states can be represented by the following equation:

$$204 \frac{\theta - \theta_r}{\theta_s - \theta_r} = \left[\frac{1}{1 + (\alpha|h|)^n} \right]^{1 - \frac{1}{n}} \quad (3)$$

205 and

$$206 K = K_s \frac{\left\{ 1 - (\alpha|h|)^{n-1} [1 + (\alpha|h|)^n]^{\frac{1}{n}-1} \right\}^2}{[1 + (\alpha|h|)^n]^{\frac{1}{2} - \frac{1}{2n}}} \quad (4)$$

207 where θ_r is the residual moisture content (%), θ_s is the saturated moisture content (%), α and n are empirical
 208 fitting parameters, α is the inverse of the air-entry pressure head, n is the pore size distribution parameter, and K_s
 209 is the saturated hydraulic conductivity (cm/s).

210 Based on the observed volumetric water content and the SWCC, the suction stress (σ^s , kPa) throughout the
 211 observation stage can be expressed as:

$$212 \sigma^s = -\frac{S_e}{\alpha} \left(S_e^{n/(1-n)} - 1 \right)^{1/n} \quad (5)$$

213 3.4 Soil water storage and drainage

214 In this study, the hydrological process of the steep slope is of utmost importance for analyzing gravitational
 215 mass wasting because of the varied soil water storage and drainage in the rainy and snow-melting seasons. Soil water
 216 is temporally stored during rainstorms, but drains after the rainstorms cease. The drainage process during melting is
 217 not addressed herein because melting water constantly contributes to high soil moisture. Therefore, soil water storage
 218 (S_s) during rainstorms and the snow-melting season and drainage (S_d) after a rainstorm ~~ceases~~ can be evaluated
 219 using the soil depth and the difference between the maximum soil moisture and antecedent soil moisture:

$$220 S_e = \frac{\theta - \theta_r}{\theta_s - \theta_r} \quad (6)$$

$$221 S_s = S_e^w \Delta h_i \quad (7)$$

$$222 S_d = P - S_e^d \Delta h \quad (8)$$

223 where S_e is the degree of saturation, θ is the in-situ observed volumetric moisture content measured (%), Δh_i is
224 the soil layer i (200 mm in this work, $i = 1, 2, 3, 4$), S_e^w and S_e^d are the residual soil moisture in the wetting and
225 drying processes (%), and P is the accumulated rainfall (mm) and equals ~~to~~ 0 mm in the snow-melting season. To
226 show the soil water storage during the rainy and snowmelt seasons, and the water drainage after rainfall, all the
227 information was considered, including rainfall amount, air temperature, soil moisture, and temperature in various
228 soil layers. The recorded rain events were categorized into four groups, ~~that is,~~ light rain, moderate rain, torrential
229 rain, and rainstorms, with rain amounts of < 10, 10–25, 25–50, and 50–100 mm, respectively.

230 4. Results

231 4.1 Erosion per unit area of gully bed and slope

232 The erosion per unit area in both bed and slope areas during the snowmelt season for Gully No. I was greater
233 than that in Gully No. II (Fig. 4). This could have been driven by the low meltwater storage and high meltwater
234 runoff at the head cut of Gully No. I. During the rainy season, the erosion per unit area for the bed of Gully No. II
235 was greater than that of Gully No. I. This may have resulted from rapid soil water storage and drainage producing
236 intensive runoff at the head cut of Gully No. II. The erosion of steep slopes is mainly due to gravitational mass
237 wasting. For Gully No. II, erosion per unit area during the snowmelt season was significantly greater than that during
238 the rainy season. During the snow-melting season, the erosion per unit area for the slope in Gully No. II was greater
239 than that in Gully No. I. Although erosion per unit area during the rainy season for Gully No. I was higher than that
240 of Gully No. II, the difference was negligible compared to that in the snow-melting season. The slopes of the
241 permanent gully were steep, and the stability of the slope primarily depended on the soil suction stress as a function
242 of the hydromechanical properties and the soil moisture.

243 As the channel bed erosion was closely correlated with the hydrological process and the slope erosion
244 corresponded to the soil suction stress, further examination of the associated soil water storage and drainage and the
245 hydromechanical properties of the soil mass in the two permanent gullies was conducted. One of the differences in
246 the hydrological processes in the head cut indicates that soil water storage and drainage occur during the rainy season.
247 Water drainage was absent during the snowmelt season. These results are due to the continuous melting of water
248 from snow and ice in macropores and fissures. Once the melting process was completed, the soil water storage
249 process ceased with the onset of the water drainage process during the transition time between the snow melting and
250 rainy seasons.

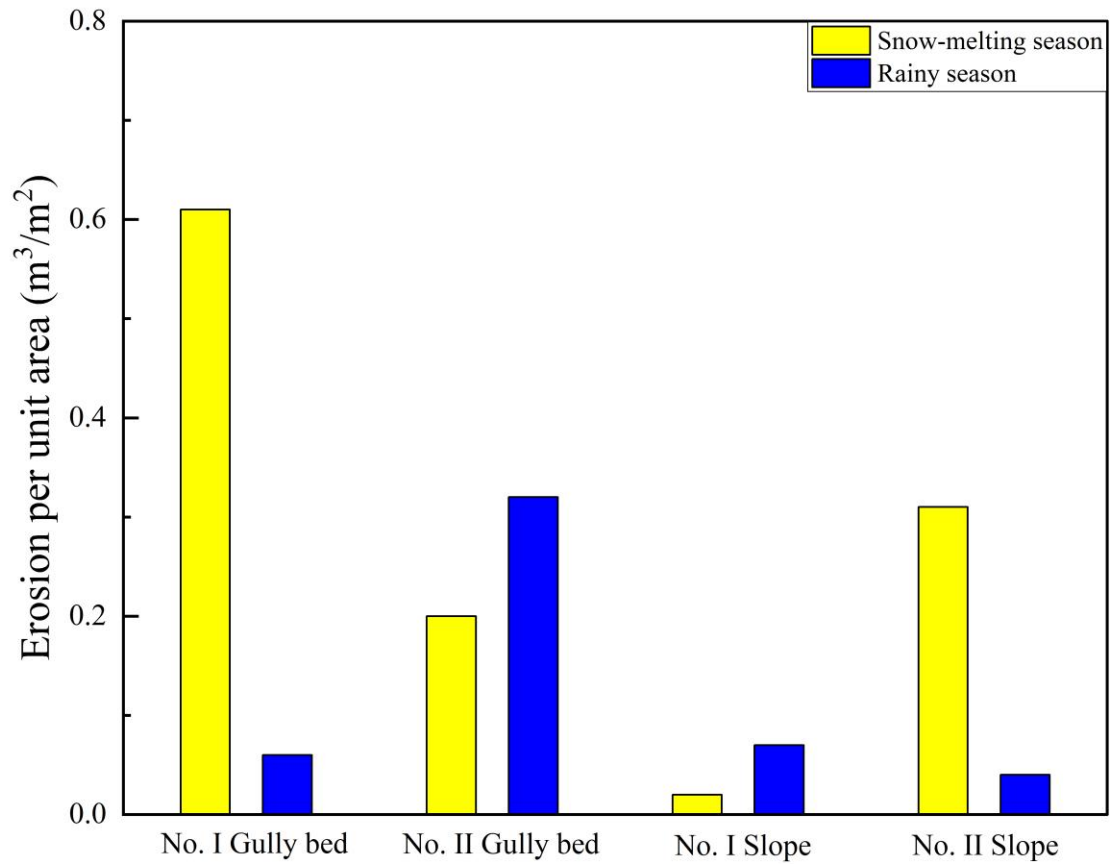


Fig. 4. Differences in the erosion per unit area for the gully bed and slope

Table 2. The physical properties and pore water pressure changes in the soil mass

Parameters	Definition	Confining pressure (kPa)	Permanent gully	
			No. I	No. II
v_{\uparrow} (kPa/min)	Pore water rising ratio	100	11.83	23.04
		200	4.86	90.52
		300	5.55	10.92
b_{\uparrow}	Pore water rising proxy as Eq. (1)	100	0.23	0.25
		200	0.24	0.46
		300	0.30	0.41
v_{\downarrow} (kPa/h)	Pore water dissipation ratio	100	3.68	22.77
		200	3.32	194.47
		300	3.66	23.94
b_{\downarrow} ($\times 10^{-5}$)	Pore water dissipation proxy as Eq. (2)	100	9.97	79.70
		200	7.80	79.40
		300	6.82	18.10
c (kPa)	Effective cohesion		11.3	7.2
φ ($^{\circ}$)	Effective friction angle		16.3	21.3
γ (kN m $^{-3}$)	Unit weight		14.1	12.5

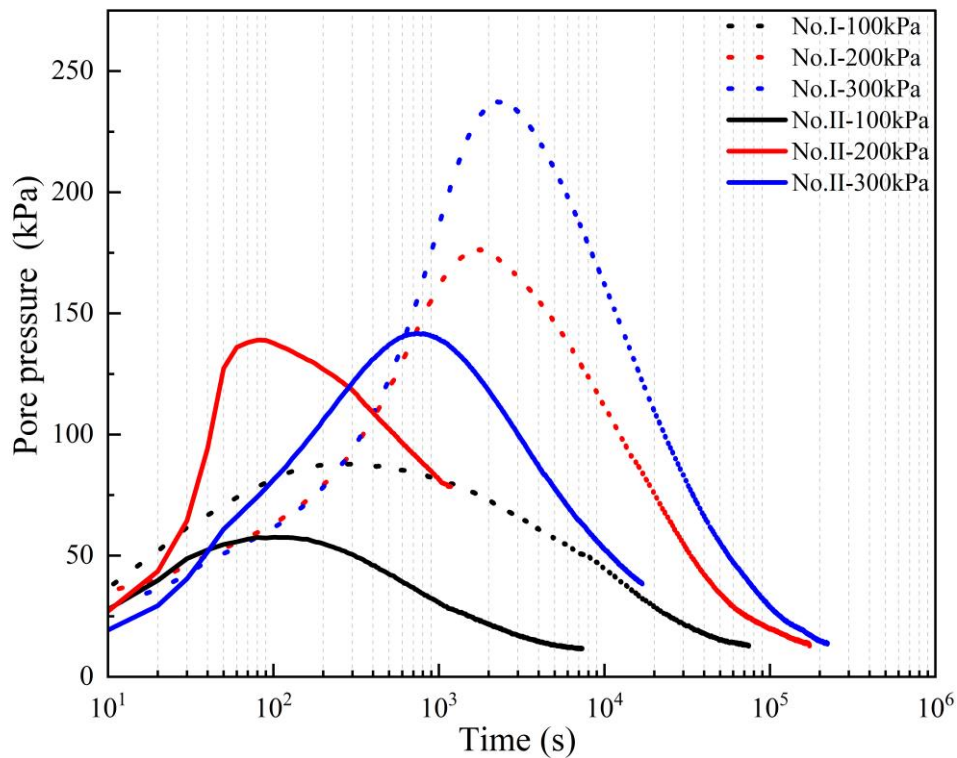
251
252
253
254

255
256
257

4.2 Physical properties of mollisols

4.2.1 Pore water pressure rising and dissipation

258 Under the same confining pressure, pronounced differences were observed in the rising and dissipation ratios
 259 of the pore water pressure within the mollisols of the two gullies. The pore water pressure results during the
 260 consolidation process at effective confining pressures of 100, 200, and 300 kPa were compared (Fig. 5). The physical
 261 properties, and the rising and dissipation ratios and proxies are listed in Table 2. The peak value of the pore water
 262 pressure within the mollisols of Gully No. I was higher than that in Gully No. II. The peak value of the pore water
 263 pressure within the mollisols of Gully No. II increased to 57.6, 139.0, and 141.7 kPa under the confining stresses of
 264 100, 200, and 300 kPa, respectively. In contrast, the peak value of the pore water pressure within the mollisols of
 265 Gully No. I increased to 87.9, 176.1, and 237.3 kPa, respectively.



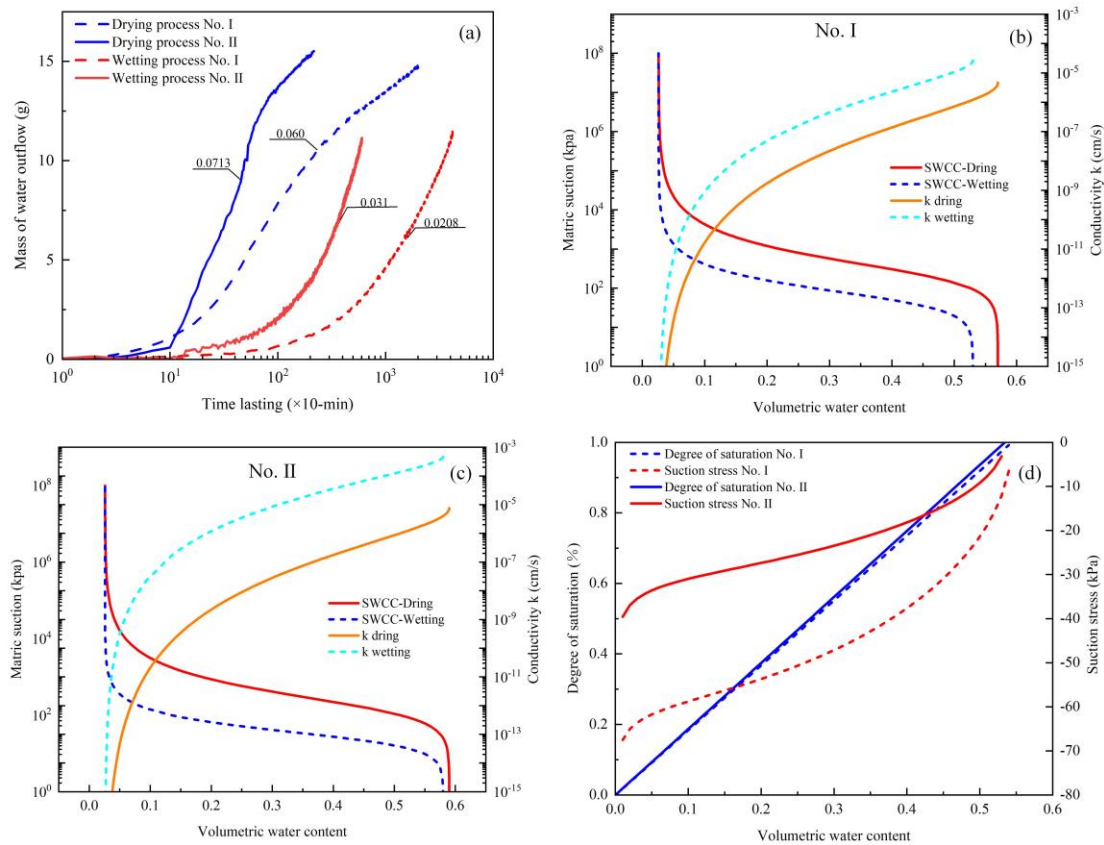
266
 267 **Fig. 5.** Variation in pore water pressure under effective confining pressure of 100, 200, and 200 kPa by GDS
 268 triaxial shear tests (GDS Instruments, UK). The proxy for the pore water pressure rising and dissipation are
 269 calculated using Eqs. (1) and (2). The rising and dissipation ratio is calculated using the pore water pressure
 270 difference during a given time interval. The values of proxy and ratio are shown in Table 2.

271 The high peak pore water pressure illustrates that the mollisols of Gully No. II had strong hydraulic conductivity
 272 as the ratio increased, and the proxy and dissipation ratio and proxy represented the pore connectivity. During the
 273 rising stage, the rising ratio of the mollisols in Gully No. II was 2 to 18.6 times greater, and its rising proxy was 1.08
 274 to 1.92 times larger than that of Gully No. I. Within the dissipation stage, the ratios were 6.20 to 58.6 greater, and
 275 its proxies were 2.65 to 8.0 times larger than those for mollisols of Gully No. I. The largest difference between these
 276 two gullies was observed under a confining stress of 200 kPa. Therefore, the increase in the pore water pressure and
 277 dissipation properties suggests that the head cut of Gully No. II may have exhibited active hydrological processes.

278
 279 **4.2.2 Hydromechanical properties of mollisols**

280 Fig. 6 shows the results of the TRIM tests, SWCC, HCF, and estimated suction stress with varying degrees of
 281 saturation. The water outflow mass was measured at 10-min intervals during the drying and wetting processes. The
 282 reason why the SWCC and HCF of the drying process and wetting process are different lies in that because water
 283 flow from the drying process relates to the applied suction level, while the water flow during the wetting process

284 was measured at a positive pressure head (Lu and Godt, 2013). The water outflow masses measured for the mollisols
 285 in Gully No. II were generally higher than those of the mollisols in Gully No. I. For the drying tests using mollisols
 286 from Gully No. II and No. I, the water outflow masses were 0.0713 and 0.060 g per 10 min, respectively. For the
 287 wetting tests, the water outflow masses were 0.031 and 0.0208 g per 10 min, respectively (Fig. 6a). Overall, the
 288 permeability of mollisol Gully No. II was higher than that of mollisol Gully No. I. The same results were obtained
 289 for the pore water pressure increase, dissipation ratio, and proxy, as shown in Table 2.



290
 291 **Fig. 6.** Differences in the hydromechanical properties of the two soil masses. (a) Water flow mass in the drying and
 292 wetting process. (b) SWCC for soil mass of permanent Gully No. I. (c) SWCC for soil mass of permanent Gully
 293 No. II. (d) Suction stress–volumetric water content curves for the two soil masses. The mass of water outflow
 294 was recorded at 10 min for each test.

295
 296 Using the parameters listed in Table 3, the SWCC and HCF curves of the mollisols were plotted (Figs. 6b and
 297 6c). Air_e-entry pressure and residual water content are two important parameters that describe the hydrological and
 298 mechanical characteristics of mollisols. The air_e-entry pressure represents the critical value at which air enters the
 299 saturated soil and begins to drain. In comparison, the values of α^d and α^w together prove that the required air_e-entry
 300 pressure for mollisols in Gully No. I was greater than that in Gully No. II, and the differences were 79.4 kPa and
 301 28.0 kPa under drying and wetting conditions, respectively (Table 3). Therefore, water infiltration into Gully No. II,
 302 during either the rainy or snow_m-melting seasons, was more active than in Gully No. I. The residual moisture did not
 303 vary markedly owing due to the similarity in the soil types similarity.

304 The saturated hydraulic conductivities of the mollisols in Gully No. I were lower than those in Gully No. II in
 305 both the drying and wetting processes. In Table 2 and Fig. 5, the pore water pressure rising ratio and proxy and the
 306 dissipation ratio and proxy further indicate that the permeability of the mollisols in Gully No. II was higher than that
 307 in the mollisols of Gully No. I. Therefore, the pore water pressure changed with varying confining stress, air_e-entry

308 pressure, and saturated hydraulic conductivities under drying and wetting conditions, suggesting that it is more
 309 challenging for the mollisols in Gully No. I to absorb and drain more water compared to mollisols in Gully No. II.

310 Figs. 6b and 6c present the matric suction and hydraulic conductivity at various soil moisture levels. However,
 311 it was ~~not-impossible~~ to compare the ~~level-of~~ suction stress level with various hydrological and mechanical
 312 parameters, as listed in Table 3. Hence, the suction stress at various soil moisture levels was determined (Fig. 6d).
 313 The absolute suction stress at the specified soil moisture for mollisols in Gully No. I was higher than that of mollisols
 314 in Gully No. II, suggesting a higher possibility of gravitational mass wasting for the mollisols in Gully No. II.

315

316 **Table 3.** Parameters describing the SWCC and the HCF from Hydrus 1D.

Parameters	Definition	Permanent gully	
		No. I	No. II
θ_r	Residual moisture	0.0262	0.0259
θ_s^d	Saturated moisture	0.57	0.59
θ_s^w		0.53	0.58
α^d (kPa ⁻¹)	The inverse of the air-entry pressure head	0.0042	0.0063
α^w (kPa ⁻¹)		0.0183	0.0375
n^d	The pore size distribution parameter	1.69	1.68
n^w		1.95	1.91
K_s^d (cm s ⁻¹)	Saturated hydraulic conductivity	4.73×10^{-6}	7.82×10^{-6}
K_s^w (cm s ⁻¹)		2.64×10^{-5}	4.26×10^{-4}

317 Notes: the superscript *d* and *w* indicate drying and wetting states.

318

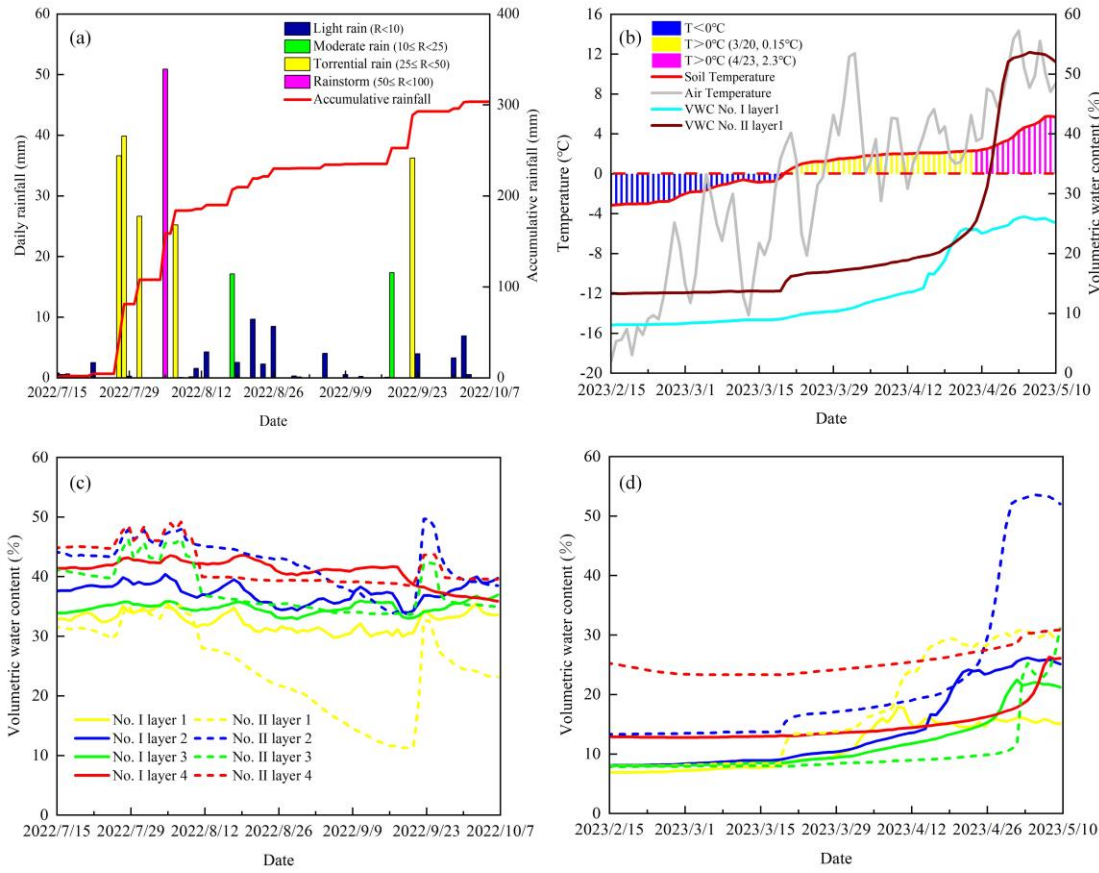
319 4.3 Hydrological response

320 4.3.1 Monitoring results

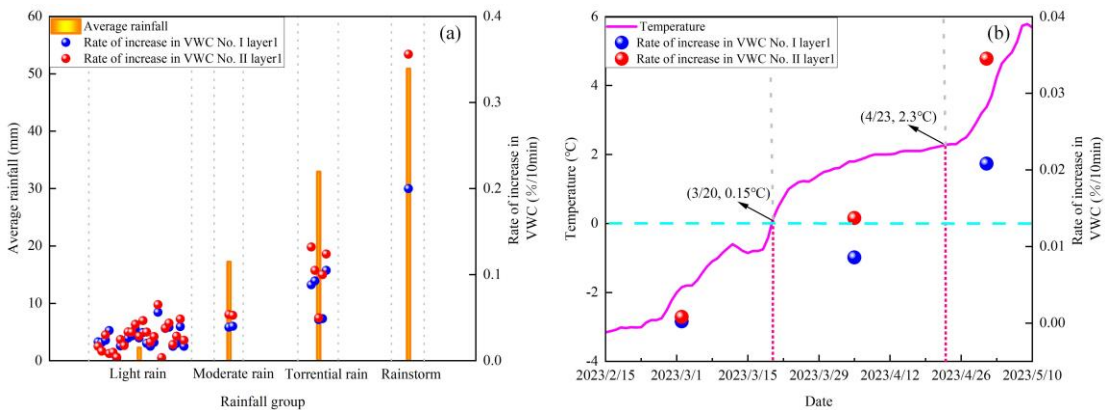
321 In total, 24 light rain events, two moderate rain events, five torrential rain events, and one rainstorm event were
 322 recorded (Fig. 7a). During the snow-melting season, the air temperature started to increase above 0 °C on March 20
 323 with an increasing gradient of 0.15 °C per day, which reached 2.3 °C per day after April 23 (Fig. 7b). For soil
 324 moisture changes, the volumetric water content at a depth of 20 cm for Gully No. II greatly increased from April 23,
 325 whereas it only slightly increased for Gully No. I. This suggests that the head cut of the Gully No. II may have
 326 experienced higher soil moisture levels. Soil moisture throughout the rainy and snowmelt seasons had dissimilarities
 327 between sites. During the rainy season, the volumetric water content at a depth of 20 cm persistently remained at a
 328 lower level of soil moisture than at the other three soil depths, as shown in Fig. 7c. However, during the snow-
 329 melting season, the volumetric water content of the 40 cm soil layer was the highest (Fig. 7d). Overall, the soil
 330 moisture content of Gully No. II, ~~in both the rainy and snowmelt seasons~~, exhibited greater fluctuations than Gully
 331 No. I ~~in both the rainy and snowmelt seasons~~. Water infiltration from rain events or snowmelt into the head cut of
 332 Gully No. II was more active than that of Gully No. I. The observed difference proves that the stored and drained
 333 water from the head cut of Gully No. II was significantly greater than that in Gully No. I.

334 To further analyze the differences in water infiltration during the rainy and snowmelt seasons, the rate of soil
 335 moisture increase at a depth of 20 cm was compared in detail (Fig. 8). Among the four types of rain events, the mean
 336 rate of increase for Gully No. II were 0.027, 0.053, 0.102, and 0.356, respectively, which were 1.12, 1.35, 1.34, and

337 1.78 larger than those for Gully No. I (Figs. 8a and 9a). During the snow-melting season, the soil moisture ratios
 338 increase ratios in the initial, medium, and final stages for Gully No. II were 3.48, 1.60, and 1.66 times, respectively,
 339 than those in Gully No. I (Fig. 8b). Therefore, the water infiltration ratios for the head cut areas of Gully No. II
 340 during the rainy and snowmelt seasons.



341 **Fig. 7.** Field-monitored rainfall conditions, air and ground temperature, and volumetric water content. (a) Rain
 342 events during the rainy season. (b) Soil, air temperature, and volumetric water content during the snow-melting
 343 season. (c) and (d) Monitored volumetric water content during the rainy season and snow-melting seasons.
 344
 345



346 **Fig. 8.** Volumetric water content increasing ratio in snow-melting ratio and the rainy season. (a) Rate of increasing
 347 increase of in VWC at varied rain events. (b) Rate of increase in VWC at three stages of temperature increase.
 348

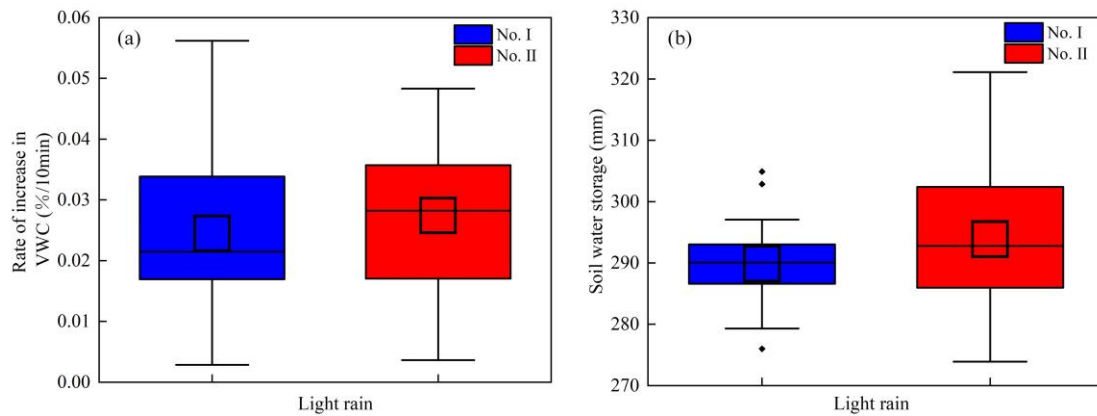


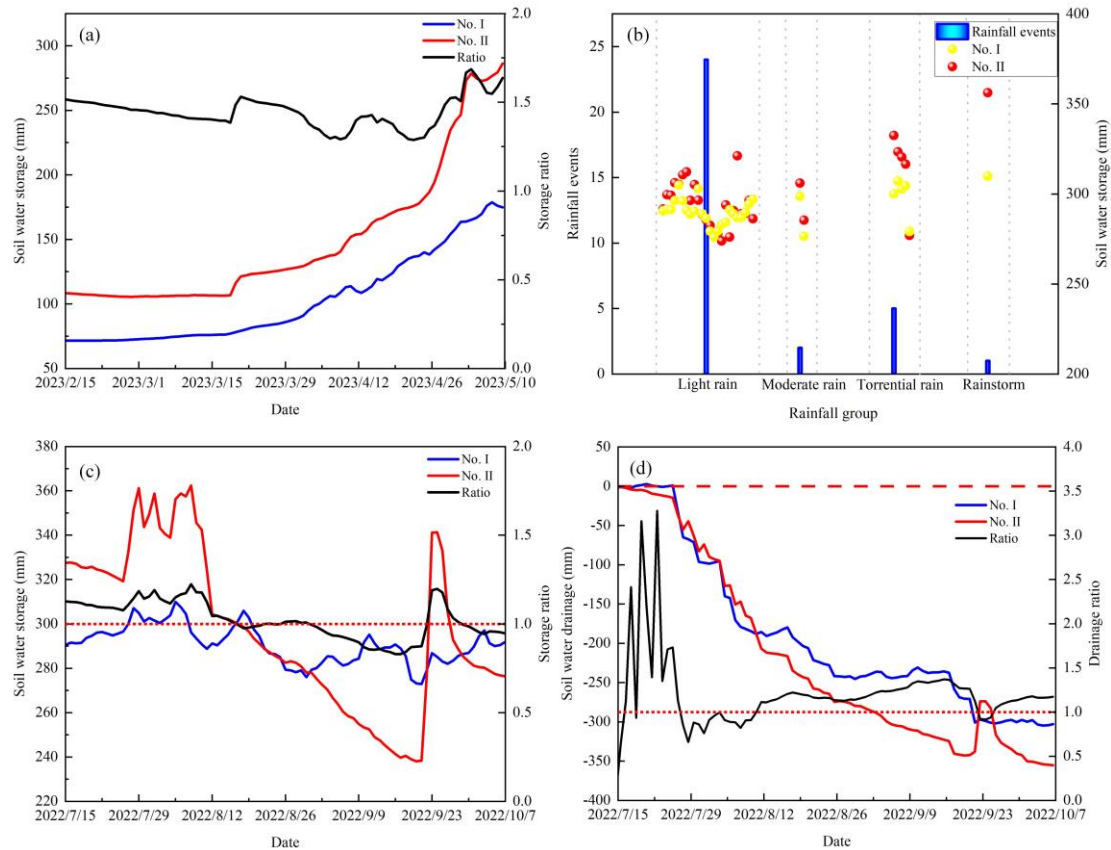
Fig. 9. Hydrologic behavior for gully head cut during light rain events. **(a)** Lower rate of increase in VWC for Gully No. I. **(b)** Higher soil water storage for Gully No. II. The three crossing lines of the boxes show the 75th quantile (Q_3), median (Q_2), and 25th quantile (Q_1) from top to bottom. The length of the box is referred to as the interquartile range ($IQR = Q_3 - Q_1$). The crossed square inside the box is the average value. The upper limit and lower limits of whiskers are $Q_3 + 1.5IQR$ and $Q_1 - 1.5IQR$, respectively. The solid squares are the outliers.

4.3.2 Soil water storage and drainage

Fig. 10 shows the stored and drained water in the soil column at the head cuts of the two gullies. During the snowmelt season, the water stored in Gully No. II was higher than that in Gully No. I. The stored water ratio was calculated by dividing the amount of water stored in Gully No. II based on the amount stored in Gully No. I was typically larger than 1.0 throughout the snowmelt season (Fig. 10a). This ratio increased abruptly from April 26. Therefore, the amount of water stored in the head cuts of Gully No. II was higher.

Regarding the four types of rain events, the mean stored water for the head cuts of Gully No. II during the 24 light rain events was greater than that in Gully No. I (Figs. 9b and 10b). The differences in water stored in the head cuts of the two gullies were 4.0, 8.1, 15.2, and 46.3 mm, respectively. Therefore, the stored water, either in the snowmelt season or rainy seasons, was higher in the head cuts of Gully No. II. However, the water stored in the head cuts of Gully No. II was not always higher than that in Gully No. I, as shown in Fig. 10c. From August 26 to September 3, 2022, the water stored at the head cut of Gully No. II was lower than that in Gully No. I. This could be attributed to high temperatures and light rain events. However, the water stored in the head cuts of Gully No. II exceeded that of Gully No. I during a torrential rainfall event on September 22. The soil water storage capacity of Gully No. II has stronger fluctuations. Rapid water infiltration generally occurs with rapid water drainage. Fig. 10d shows the water drainage and drainage ratios of the two gullies during the rainy season. The water drained from Gully No. II was higher than that in Gully No. I. Therefore, the head cut area of the Gully No. II had better soil water storage capability in snowmelt and rainy seasons and more rapid water drainage in the rainy season than Gully No. I.

In summary, rapid soil water storage and drainage for the head cuts of Gully No. II during torrential rain or rainstorms coincided with both the observed pore water pressure rise and dissipation and the hydromechanical properties of mollisols. The high permeability of mollisols at the head cut of Gully No. II was attributed to more rapid soil water storage, drainage processes, and stored water. This could have a considerable influence on the erosion intensity of the steep slope and gully bed of the permanent gully.



380
 381 **Fig. 10.** Hydrological response during the rainy and snow-melting season. **(a)** Soil water storage and the storage
 382 ratio during the snow-melting season. **(b)** Soil water storage at varied rain events. **(c)** Soil water storage and
 383 the storage ratio for the two permanent gullies. **(d)** Soil water drainage and the drainage ratio during the rainy
 384 season. During the rainy season, soil water storage and drainage synchronously change with the onset and end
 385 of rainfall.

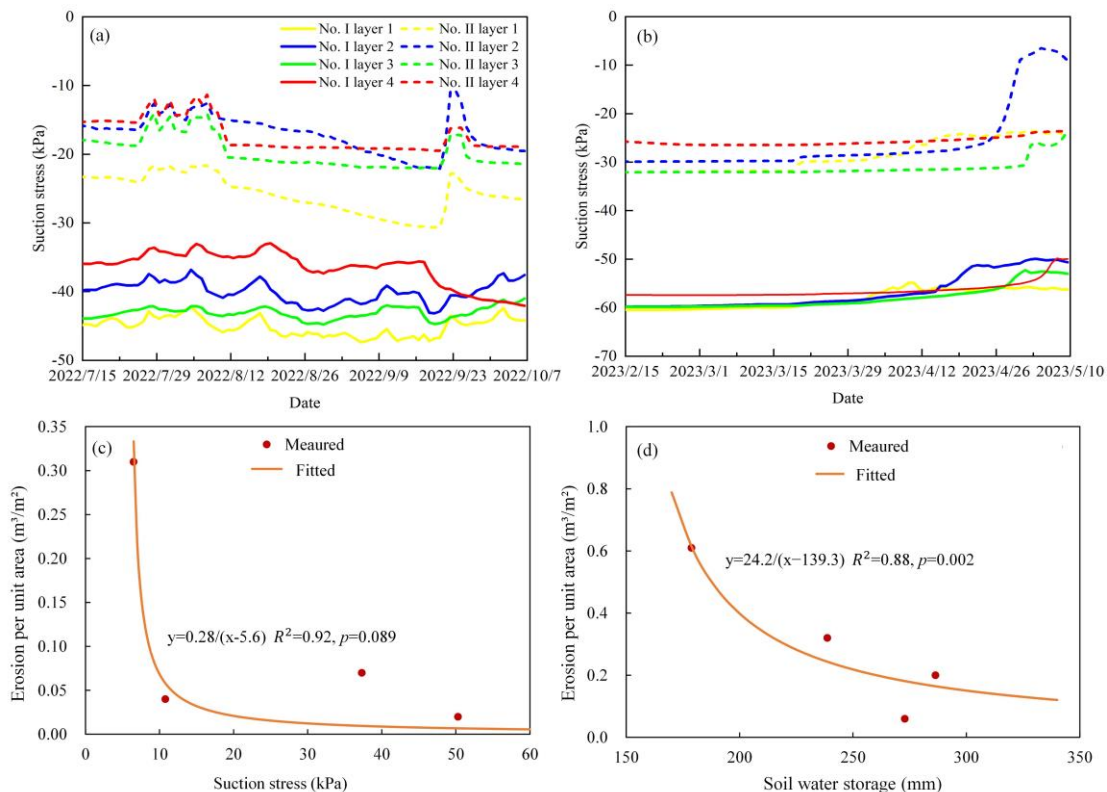
386 387 388 **4.4 Hydromechanical response and soil loss**

389 As for the mollisols in the head cut area of the two permanent gullies differed in hydromechanical properties, so
 390 the monitored soil moisture varied greatly in the field. The suction stress was estimated according to the field-
 391 monitored soil moisture at each site and the relationship between the soil moisture and matric suction (Figs. 6d, 7c,
 392 and 7d). During the rainy season, the absolute value of the suction stress of the mollisols in Gully No. II was lower
 393 than that of Gully No. I (Fig. 11a). The smaller absolute values of the suction stress for the mollisols of Gully No. II
 394 during the snowmelt season (Figure 11b). Moreover, the smaller suction stress in the snowmelt season may have
 395 resulted in strong erosion on the slope of Gully No. II, as shown in Fig. 4.

396 As the hydrological process of the head cut area is closely related to channel bed erosion, the hydromechanical
 397 response influences slope stability. It is important to analyze the possible relationship between the erosion per unit
 398 area on the channel bed, soil water storage, and erosion of a steep slope with suction stress. In general, a high
 399 absolute value of the suction stress is associated with strong cohesive forces between the soil particles, which is a
 400 sign of stability. In contrast, a low absolute value of suction stress suggests a higher potential for slope failure.
 401 Therefore, the relationship between the absolute value of the suction stress and erosion per unit area could be
 402 negative. Fig. 11c shows the reciprocal relationship between the suction stress and erosion per unit area of the slope.
 403 The empirical relationship indicates that gravitational mass wasting occurred on the slope, and the permanent gully

404 expanded when the suction stress remained relatively low for a prolonged period, particularly at approximately 5.6
 405 kPa for the study area.

406 Erosion of the channel bed is closely related to runoff discharge during erosive rain events. During erosive rain
 407 events, the amount of stored soil water decreases runoff amount and intensity. The less rainwater stored during
 408 erosive rain events, the higher the runoff amount, or the more intensive the channeled flow. Therefore, the
 409 relationship between the soil water storage and erosion per unit area of the channel bed could be negative. Fig. 11d
 410 shows the reciprocal relationship between erosion per unit area of the channel bed and soil water storage. It indicates
 411 that excessive rainwater in erosive rain events could create intensified channeled flow to erode the channel bed if
 412 the stored water in the mollisols reached a threshold, such as 139.3 mm, in this study area.



413
 414 **Fig. 11.** Relationship between hydrology and the hydromechanical state with the erosion per unit area over
 415 approximately 3 months. **(a)** Suction stress during the rainy season. **(b)** Suction stress during the snow-melting
 416 season. **(c)** erosion per unit area on the slope decreases with suction stress. **(d)** The erosion per unit area on the
 417 channel bed decreases with the amount of soil water storage-amount. The time for the monitored rainy and
 418 melting seasons were 111 d and 97 d.

419 5 Discussion

420 The physical processes of permanent gully development can be categorized into gravitational mass wasting on
 421 steep slopes and sediment delivery on channel beds (Montgomery and Dietrich, 1992; van Beek et al., 2008; Luffman
 422 et al., 2015). Traditionally, most studies on gully erosion have focused on soil loss owing to water erosion and piping.
 423 Soil loss estimation is typically determined by several primary factors, such as the upslope contributing area,
 424 topographic conditions, erosive rainfall factors, and land use conditions (Li et al., 2015; Xu et al., 2017; Wang et al.,
 425 2021; Tang et al., 2022). The physical mechanics of bed erosion and slope erosion are different, making it
 426 challenging to accurately predict soil loss on steep slopes. The gravitational mass-wasting process on a slope differs
 427 from that of rainfall-induced shallow landslides, especially for those without failure planes (Poesen et al., 1998; Guo

et al., 2020). However, they share similarities, such as ~~a decrease in~~ soil strength due to water infiltration (Guo et al., 2019). Thus, a thorough mechanical analysis is necessary to understand the physical processes of gravitational mass wasting on the slope and sediment delivery on the channel bed.

This study thoroughly investigated the effects of hydrological factors and hydromechanical properties on soil loss on both slopes and channel beds. Mass failure on the hillslopes was governed by suction stress. Meanwhile, erosion on the channel beds was influenced by the soil water storage or runoff amount. Therefore, hydrological factors related to soil water storage and drainage were analyzed (Fig. 10), along with volumetric changes at various rain events and snow-melting stages (Fig. 8). In this study, we also investigated the hydromechanical properties and pore water pressure at a given confining stress (Table 2 and Fig. 5), the relationship between the saturation degree and suction stress (Fig. 6), and estimated the suction stress variation during the rainy and snow-melting seasons (Figs. 11a and 11b). Field observations revealed two permanent gullies with distinct erosion on the slope and gully beds. Gully No. II shows signs of head cut disruption, in contrast to Gully No. I, resulting in disparities in erosion per unit area for both seasons and sites. The hydromechanical properties of the mollisols are distinct between the two gullies, directly affecting water movement. This is evident from the increase in pore water pressure, dissipation ratio, and proxy. In the head cut of Gully No. II, the mollisols were significantly disturbed, and the soil mass had higher permeability and lower suction stress at a given saturation degree. This finding indicates more active water infiltration compared to Gully No. I was triggered by changes in the soil's capacity to store and release water and the higher volumetric water content increasing ratio. Therefore, the head cut area of Gully No. II underwent more aggressive hydrological processes. Additionally, the observed rainfall amount of 139.3 mm in this study was smaller than the 177 mm proposed by Tang et al. (2023). This could be explained by the different capacities for plant interception and depression detention during the rainy season.

The soil water storage and drainage capacity at the head cut considerably influenced soil loss. Although this study focused primarily on soil water storage and its impact, runoff was not addressed. The soil water storage and runoff depth were approximately equal to the rainfall depth from the water balance perspective ~~of water balance~~. Consequently, the erosion per unit area of the channel bed was inversely proportional to the soil water storage, as shown in Fig. 11d. Some researchers have identified factors leading to the erosion of mass failures on steep slopes, such as long-duration storms (Xu et al., 2020), initial soil moisture in the pre-winter season (Wen et al., 2024), presence of tensile crack morphology (Zhou et al., 2023) and heaving and thawing (Thomas et al., 2009). The head cut of Gully No. II has a high level of disturbance, which may result in higher permeability, quicker water pressure response, and higher soil moisture during ~~either~~ the rainy or snowmelt seasons. Meanwhile, the soil suction stress was lower, and slope erosion was more intense than that of Gully No. I. The distance between the two gullies was only 1.4 km, and the climatic conditions were similar. Therefore, soil properties may be the dominant intrinsic factors governing soil loss on gully slopes.

Commonly, the gully bed erosion rates mainly depend on runoff intensity, and some ~~studies~~ studies found reported that the runoff hydraulics ~~of runoff~~ in the rainy season ~~was~~ were significantly higher than the snow-melting ~~melting~~ runoff. However, ~~some additional~~ studies also proved that gully heads may retreat faster in the snow-melting season than in the summer (Wu et al., 2008; Hu et al., 2009). ~~In fact,~~ the accumulated snowfall depth during the monitoring duration in this ~~work study~~ work study was high, up to 49.6 mm, which was far more than the average snow depth of 30 mm. Besides, the snowfall ~~was~~ melted all during from 3 to 10 May 2023 (Figs. 7a and 7b). Therefore, heavy snowfall during the winter of 2022 and early spring of 2023 and the intensive melting may result in ~~the~~ high soil moisture, and intensive runoff, ultimately causing ~~to cause strong~~ substantial bed erosion. Long-term saturation during the snowmelt season provides sufficient water infiltration and low suction stress. Therefore, the highest erosion per unit area occurred in the snowmelt season, but not in the rainy season.

Dong et al. (2011) revealed that a critical mass water content for gravitational mass wasting ranged from 31.0%

472 to 33.8%, corresponding to a volumetric water content of 39.0% to 48.0% for the soil mass and a suction stress of
473 11.0 kPa. This showed that the direct-shear apparatus limited the ability to differentiate between the effective
474 cohesion and suction stress contributions to total cohesion. As shown in Fig. 10b and supported by Xu et al. (2020),
475 the high soil water storage during the snow-melting season in Gully No. II (Fig. 9a) and long-term water infiltration
476 can ~~result in~~ lower suction stress and higher erosion per unit area. This suggests a potentially reciprocal relationship
477 between the absolute suction stress and erosion per unit area. The result shown in Figs. 11c and 11d ~~is-are~~ key
478 findings and main contributions in the study domain of gully erosion, as ~~it-they clearly clarifies~~ the role of suction
479 stress of stored water on soil loss from steep slopes and gully bedbeds, respectively. ~~It also~~ Our results also tells the
480 ~~truth imply~~ that the soil water storage ~~couldn't may not~~ equal ~~to the~~ amount of event rainfall ~~from the event amount~~,
481 but instead partially derives from the initial soil water. ~~In fact, f~~ Figure 11 ~~specialy illustrate~~ illustrates that antecedent
482 soil moisture or precipitation substantially have influences on surface runoff depth and soil loss during the permanent
483 gully expansion in MEC, while this important-critical aspect has been neglected in previous study. In other words,
484 the effect of antecedent precipitation would-should be assessed in predicting soil loss as it closely relates to the soil
485 water and generate indirectly influences on the runoff generation and intensity (Sachs and Sarah, 2017; Wei et al.,
486 2017; Schoener and Stone, 2019; Wang et al., 2019). ~~Importantly~~ Notably, the theoretical framework ideology
487 underlying of this work ~~adopts-is the theory frame~~ that the soil loss at the steep slopes occurs by-through the
488 mechanism of bank slope stability, and the loss in the gully beds occurs on-due to condition that the balance between
489 the shear force from runoff water ~~to-and~~ soil erodibility. Therefore, it is better-preferrable way to predict ~~the~~ soil loss
490 in the permanent gullies from ~~both~~ soil water storage and the hydromechanical response of soil mass, ~~other-rather~~
491 than solely from rainfall amount.

492 6 Conclusions

493 Permanent gully development is a hydrogeomorphic phenomenon, and its physical mechanics can be attributed
494 to the hydrological and hydromechanical responses of the head cut. In the mollisol region of Northeast China,
495 numerous studies on gully development have focused on soil loss in response to rainfall or snow depth. However,
496 ~~to-date~~, relatively few studies have addressed the physical mechanics of gravitational mass wasting. This study has
497 provided a complete analysis of soil loss on steep slopes and channel beds in two permanent gullies according to
498 hydrological processes, such as infiltration, soil water storage, ~~and~~ drainage, and hydromechanical responses, such
499 as changes in suction stress levels. The following conclusions were drawn:

500 (1) Mollisols in the head-head-cut areas of Gully No. II exhibited a higher permeability than Gully No. I. This
501 can be attributed to the elevated ratio and proxy for pore water pressure rise and dissipation. The TRIM test results
502 confirmed that the saturated mollisols in the Gully No. II drain faster than Gully No. I, owing to their higher air-
503 entry pressure and saturated hydraulic conductivity during the wetting and drying cycles.

504 (2) The head cut area of Gully No. II exhibited more intense hydrological processes than Gully No. I. This
505 could be explained by the higher ratio of soil moisture increase observed during the four rain event types and three
506 snow-melting stages. Soil water storage in Gully No. II experienced greater fluctuations during torrential rains and
507 rainstorms. Overall, the absolute suction in Gully No. II remained lower than that in Gully No. I, potentially
508 triggering greater erosion on the steep slopes.

509 (3) The relationships between erosion per unit area on the steep slope and channel bed were analyzed for the
510 suction stress and soil water storage. Our findings indicate that low suction stress and high soil water storage can
511 ~~lead-to~~ increased gravitational mass wasting while reducing erosion on the channel bed. The two empirical
512 relationships and their efficiency can be improved-enhanced by incorporating data from ongoing monitoring efforts
513 to enhance the prediction of future soil loss.

514

515 **Acknowledgements**

516 ~~All authors declare that no conflict of interest exists.~~ This work ~~was study~~ was supported by the National Key
517 Research and Development Program (Grant No. 2021YFD1500700). The authors extend their gratitude to the
518 colleges at the Jiusan Soil and Water Conservation Experimental Station, Beijing Normal University, for their help
519 during field investigations.

520

521 **Code/ and dData availability**

522 ~~Any readers can contact~~ The corresponding author, Prof. Chao Ma, ~~as the corresponding author~~ is willing to share
523 the raw/processed data- upon reasonable request.

524

525 **Author contributions**

526 Prof. Ma ~~launched conceived this the work study~~ based on his skills in gravitational mass-wasting and unsaturated
527 soil mechanics, and proposed the ~~idea ology concept~~ of hydrology and hydro~~mechanical-mechanical~~ conditions in
528 analyzing ~~the~~ gravitational mass-wasting. Under the guidance of Prof. Ma, Mr. Dongshuo Zheng and Shoupeng
529 Wang ~~finished-conducted~~ indoor tests of soil strength and hydraulic-mechanical properties. Prof. Zhang helped
530 determine the field observation sites. Dr. Dong gave insightful comments. Dr. Jie Tang and Yanru Wen provided the
531 research progress about the gravitational mass-~~wasting~~ on gully expansion in the study area.

532

533 **Competing interests**

534 ~~All~~ The authors ~~have declared that there were~~ no conflicts of interests ~~and competing interests~~.

535

536 **References**

- 537 [1] Allen, P. M., Arnold, J. G., Auguste, L., White, J., and Dunbar, J.: Application of a simple headcut advance
538 model for gullies, *Hydrol. Earth Syst. Sci.*, 43, 202-217, <https://doi.org/10.1002/esp.4233>, 2018.
- 539 [2] Bierman, P. R. and Montgomery, D. R.: Key Concepts in Geomorphology, W. H. Freeman and Company
540 Publishers, ISBN 13:9781429238601, 2014.
- 541 [3] Dong, Y., Wu, Y., Yin, J., Wang, Y., and Gou, S.: Investigation of Soil Shear-Strength Parameters and
542 Prediction of the Collapse of Gully Walls in the Black Soil Region of Northeastern China, *Phys. Geogr.*, 32,
543 161-178, <https://doi.org/10.2747/0272-3646.32.2.161>, 2011.
- 544 [4] Dong, Y., Wu, Y., Qin, W., Guo, Q., Yin, Z., and Duan, X.: The gully erosion rates in the black soil region of
545 northeastern China: Induced by different processes and indicated by different indexes, *Catena*, 182,
546 <https://doi.org/10.1016/j.catena.2019.104146>, 2019.
- 547 [5] Evans, D.: *Geomorphology: Critical Concepts in Geography - Volume IV, Glacial Geomorphology*, Routledge.,
548 ISBN 9780415641708, 2004.
- 549 [6] Fan, H., Hou, Y., Xu, X., Mi, C., and Shi, H.: Composite Factors during Snowmelt Erosion of Farmland in
550 Black Soil Region of Northeast China: Temperature, Snowmelt Runoff, Thaw Depths and Contour Ridge
551 Culture, *Water*, 15, <https://doi.org/10.3390/w15162918>, 2023.
- 552 [7] Farkas, C., Randriamampianina, R., and Majercak, J.: Modelling impacts of different climate change scenarios
553 on soil water regime of a Mollisol, *Cereal Res. Commun.*, 33, 185-188,
554 <https://doi.org/10.1556/crc.33.2005.1.45>, 2005.

- 555 [8] Gómez-Gutiérrez, A., Schnabel, S., De Sanjosé, J. J., and Contador, F. L.: Exploring the relationships between
556 gully erosion and hydrology in rangelands of SW Spain, *Z. Geomorphol*, 56, 27-44,
557 <https://doi.org/10.1127/0372-8854/2012/s-00071>, 2012.
- 558 [9] Guan, Y., Yang, S., Zhao, C., Lou, H., Chen, K., Zhang, C., and Wu, B.: Monitoring long-term gully erosion
559 and topographic thresholds in the marginal zone of the Chinese Loess Plateau, *Soil Tillage Res.*, 205,
560 <https://doi.org/10.1016/j.still.2020.104800>, 2021.
- 561 [10] Guo, W., Xu, X., Wang, W., Zhu, T., and Liu, Y.: Experimental study of shallow mass movements on gully
562 slopes and associated sediment under rainfall on the Chinese loess plateau, *Geomorphology*, 350,
563 <https://doi.org/10.1016/j.geomorph.2019.106919>, 2020.
- 564 [11] Guo, W., Luo, L., Wang, W., Liu, Z., Chen, Z., Kang, H., and Yang, B.: Sensitivity of rainstorm-triggered
565 shallow mass movements on gully slopes to topographical factors on the Chinese Loess Plateau,
566 *Geomorphology*, 337, 69-78, <https://doi.org/10.1016/j.geomorph.2019.04.006>, 2019.
- 567 [12] Harmon, R. S. and Doe, W. W.: *Landscape erosion and evolution modeling*, Springer Science + Business Media,
568 New York., ISBN 978-1-4613-5139-9, 2001.
- 569 [13] Hu, G., Wu, Y., Liu, B., Yu, Z., You, Z., and Zhang, Y.: Short-term gully retreat rates over rolling hill areas in
570 black soil of Northeast China, *Catena*, 71, 321-329, <https://doi.org/10.1016/j.catena.2007.02.004>, 2007.
- 571 [14] Hu, G., Wu, Y., Liu, B., Zhang, Y., You, Z., and Yu, Z.: The characteristics of gully erosion over rolling hilly
572 black soil areas of Northeast China, *J Geogr Sci.*, 19, 309-320, <https://doi.org/10.1007/s11442-009-0309-4>, 2009.
- 573 [15] Hayas, A., Peña, A., and Vanwallegem, T.: Predicting gully width and widening rates from upstream
574 contribution area and rainfall: A case study in SW Spain, *Geomorphology*, 341, 130-139,
575 <https://doi.org/10.1016/j.geomorph.2019.05.017>, 2019.
- 576 [16] Jiao, J., Qin, W., Li, K., Xu, H., Yin, Z., and Hou, S.: Critical thresholds for stage division of water erosion
577 process in different ridge systems in mollisol region of Northeast China, *J Mt. Sci.*, 20, 1540-1560,
578 <https://doi.org/10.1007/s11629-022-7476-5>, 2023.
- 579 [17] Kirkby, M. J. and Bracken, L. J.: Gully processes and gully dynamics, *Earth Surf. Process. Landf.*, 34, 1841-
580 1851, <https://doi.org/10.1002/esp.1866>, 2009.
- 581 [18] Li, H., Cruse, R. M., Liu, X., and Zhang, X.: Effects of Topography and Land Use Change on Gully
582 Development in Typical Mollisol Region of Northeast China, *Chin. Geogr. Sci.*, 26, 779-788,
583 <https://doi.org/10.1007/s11769-016-0837-7>, 2016.
- 584 [19] Li, H., Shen, H., Wang, Y., Wang, Y., and Gao, Q.: Effects of Ridge Tillage and Straw Returning on Runoff
585 and Soil Loss under Simulated Rainfall in the Mollisol Region of Northeast China, *Sustainability*, 13,
586 <https://doi.org/10.3390/su131910614>, 2021.
- 587 [20] Li, Z., Zhang, Y., Zhu, Q., He, Y., and Yao, W.: Assessment of bank gully development and vegetation coverage
588 on the Chinese Loess Plateau, *Geomorphology*, 228, 462-469,
589 <https://doi.org/10.1016/j.geomorph.2014.10.005>, 2015.
- 590 [21] Li, Z., Zhang, Y., Zhu, Q., Yang, S., Li, H., and Ma, H.: A gully erosion assessment model for the Chinese
591 Loess Plateau based on changes in gully length and area, *Catena*, 148, 195-203,
592 <https://doi.org/10.1016/j.catena.2016.04.018>, 2017.
- 593 [22] Liu, X., Guo, M., Zhang, X., Zhang, S., Zhou, P., Chen, Z., Qi, J., and Shen, Q.: Morphological characteristics
594 and volume estimation model of permanent gullies and topographic threshold of gullying in the rolling hilly
595 Mollisols region of northeast China, *Catena*, 231, <https://doi.org/10.1016/j.catena.2023.107323>, 2023.
- 596 [23] Lu, N. and Godt, J. W.: *Hillslope Hydrology and Stability*, Cambridge University Press, Cambridge,
597 <https://doi.org/10.1017/CBO9781139108164>, 2013.
- 598 [24] Luffman, I. E., Nandi, A., and Spiegel, T.: *Gully morphology, hillslope erosion, and precipitation*

- 599 characteristics in the Appalachian Valley and Ridge province, southeastern USA, *Catena*, 133, 221-232,
600 <https://doi.org/10.1016/j.catena.2015.05.015>, 2015.
- 601 [25] Montgomery, D. R. and Dietrich, W. E.: Channel initiation and the problem of landscape scale, *Science*, 255,
602 826-830, <https://doi.org/10.1126/science.255.5046.826>, 1992.
- 603 [26] Mualem, Y.: Hysteretical models for prediction of the hydraulic conductivity of unsaturated porous media,
604 *Water Resour. Res.*, 12, 1248-1254, <https://doi.org/10.1029/WR012i006p01248>, 1976.
- 605 [27] Poesen, J., Vandaele, K., and van Wesemael, B.: Gully Erosion: Importance and Model Implications. In:
606 Boardman, J., Favis-Mortlock, D. (eds) *Modelling Soil Erosion by Water*. NATO ASI Series, vol 55. Springer,
607 Berlin, Heidelberg., https://doi.org/10.1007/978-3-642-58913-3_22, 1998.
- 608 [28] Poesen, J. W. A., Torri, D. B., and Vanwallegghem, T.: Gully Erosion: Procedures to Adopt When Modelling
609 Soil Erosion in Landscapes Affected by Gullyng, in: *Handbook of Erosion Modelling*, 360-386,
610 <https://doi.org/10.1002/9781444328455.ch19>, 2010.
- 611 [29] Rengers, F. K. and Tucker, G. E.: Analysis and modeling of gully headcut dynamics, North American high
612 plains, *J. Geophys. Res.-Earth Surf.*, 119, 983-1003, <https://doi.org/10.1002/2013jf002962>, 2014.
- 613 [30] Stein, O. R. and Latray, D. A.: Experiments and modeling of head cut migration in stratified soils, *Water*
614 *Resour. Res.*, 38, 1284, <https://doi.org/10.1029/2001WR001166>, 2002.
- 615 [31] Sidle, R. C., Gomi, T., Usuga, J. C. L., and Jarihani, B.: Hydrogeomorphic processes and scaling issues in the
616 continuum from soil pedons to catchments, *Earth Sci. Rev.*, 175, 75-96,
617 <https://doi.org/10.1016/j.earscirev.2017.10.010>, 2017.
- 618 [32] Svoray, T., Michailov, E., Cohen, A., Rokach, L., and Sturm, A.: Predicting gully initiation: comparing data
619 mining techniques, analytical hierarchy processes and the topographic threshold, *Earth Surf. Process. Landf.*,
620 37, 607-619, <https://doi.org/10.1002/esp.2273>, 2012.
- 621 [33] Sachs, E. and Sarah, P.: Combined effect of rain temperature and antecedent soil moisture on runoff and
622 erosion on Loess, *Catena*, 158, 213-218, <https://doi.org/10.1016/j.catena.2017.07.007>, 2017.
- 623 [34] Schoener, G. and Stone, M. C.: Impact of antecedent soil moisture on runoff from a semiarid catchment, *J*
624 *Hydrol.*, 569, 627-636, <https://doi.org/10.1016/j.jhydrol.2018.12.025>, 2019.
- 625 [35] Tang, J., Xie, Y., Wu, Y., and Liu, G.: Influence of precipitation change and topography characteristics on the
626 development of farmland gully in the black soil region of northeast China, *Catena*, 224,
627 <https://doi.org/10.1016/j.catena.2023.106999>, 2023.
- 628 [36] Tang, J., Xie, Y., Liu, C., Dong, H., and Liu, G.: Effects of rainfall characteristics and contour tillage on
629 ephemeral gully development in a field in Northeastern China, *Soil Tillage Res.*, 218,
630 <https://doi.org/10.1016/j.still.2021.105312>, 2022.
- 631 [37] Tang, J., Liu, G., Xie, Y., Duan, X., Wang, D., and Zhang, S.: Ephemeral gullies caused by snowmelt: A ten-
632 year study in northeastern China, *Soil Tillage Res.*, 212, 105048, <https://doi.org/10.1016/j.still.2021.105048>,
633 2021.
- 634 [38] Tebebu, T. Y., Abiy, A. Z., Zegeye, A. D., Dahlke, H. E., Easton, Z. M., Tilahun, S. A., Collick, A. S., Kidnau,
635 S., Moges, S., Dadgari, F., and Steenhuis, T. S.: Surface and subsurface flow effect on permanent gully
636 formation and upland erosion near Lake Tana in the northern highlands of Ethiopia, *Hydrol. Earth Syst. Sci.*,
637 14, 2207-2217, <https://doi.org/10.5194/hess-14-2207-2010>, 2010.
- 638 [39] Thomas, J. T., Iverson, N. R., and Burkart, M. R.: Rank-collapse processes in a valley-bottom gully, western
639 Iowa, *Earth Surf. Process. Landf.*, 34, 109-122, <https://doi.org/10.1002/esp.1699>, 2009.
- 640 [40] Torri, D. and Poesen, J.: A review of topographic threshold conditions for gully head development in different
641 environments, *Earth Sci. Rev.*, 130, 73-85, <https://doi.org/10.1016/j.earscirev.2013.12.006>, 2014.
- 642 [41] van Beek, R., Cammeraat, E., Andreu, V., Mickovski, S. B., and Dorren, L.: Hillslope Processes: Mass Wasting,

- 643 Slope Stability and Erosion, in: Slope Stability and Erosion Control: Ecotechnological Solutions, edited by:
644 Norris, J. E., Stokes, A., Mickovski, S. B., Cammeraat, E., van Beek, R., Nicoll, B. C., and Achim, A., Springer
645 Netherlands, Dordrecht, 17-64, https://doi.org/10.1007/978-1-4020-6676-4_3, 2008.
- 646 [42] van Genuchten, M. T.: A Closed-form Equation for Predicting the Hydraulic Conductivity of Unsaturated Soils,
647 Soil Sci. Soc. Am. J., 44, 892-898, <https://doi.org/10.2136/sssaj1980.03615995004400050002x>, 1980.
- 648 [43] Vanmaercke, M., Poesen, J., Van Mele, B., Demuzere, M., Bruynseels, A., Golosov, V., Bezerra, J. F. R.,
649 Bolysov, S., Dvinskih, A., Frankl, A., Fuseina, Y., Guerra, A. J. T., Haregeweyn, N., Ionita, I., Imwangana, F.
650 M., Moeyersons, J., Moshe, I., Samani, A. N., Niacsu, L., Nyssen, J., Otsuki, Y., Radoane, M., Rysin, I.,
651 Ryzhov, Y. V., and Yermolaev, O.: How fast do gully headcuts retreat?, Earth Sci. Rev, 154, 336-355,
652 <https://doi.org/10.1016/j.earscirev.2016.01.009>, 2016.
- 653 [44] Wei, L., Zhang, B., and Wang, M.: Effects of antecedent soil moisture on runoff and soil erosion in alley
654 cropping systems, Agr Water Manage., 94, 54-62, <https://doi.org/10.1016/j.agwat.2007.08.007>, 2007.
- 655 [45] Wu, Y., Zheng, Q., Zhang, Y., Liu, B., Cheng, H., and Wang, Y.: Development of gullies and sediment
656 production in the black soil region of northeastern China, Geomorphology, 101, 683-691,
657 <https://doi.org/10.1016/j.geomorph.2008.03.008>, 2008.
- 658 [46] Wang, J., Zhang, Y., Deng, J., Yu, S., and Zhao, Y.: Long-Term Gully Erosion and Its Response to Human
659 Intervention in the Tableland Region of the Chinese Loess Plateau, Remote Sens., 13,
660 <https://doi.org/10.3390/rs13245053>, 2021a.
- 661 [47] Wang, L., Zheng, F., Liu, G., Zhang, X., Wilson, G. V., Shi, H., and Liu, X.: Seasonal changes of soil erosion
662 and its spatial distribution on a long gentle hillslope in the Chinese Mollisol region, Int. Soil Water Conserv.
663 Res., 9, 394-404, <https://doi.org/10.1016/j.iswcr.2021.02.001>, 2021b.
- 664 [48] Wang, Z., Liu, B., Wang, X., Gao, X., and Liu, G.: Erosion effect on the productivity of black soil in Northeast
665 China, Sci. China Ser. D-Earth Sci., 52, 1005-1021, <https://doi.org/10.1007/s11430-009-0093-0>, 2009.
- 666 [49] Wayllace, A. and Lu, N.: A Transient Water Release and Imbibitions Method for Rapidly Measuring Wetting
667 and Drying Soil Water Retention and Hydraulic Conductivity Functions, Geotech. Test. J., 35, 103-117,
668 <https://doi.org/10.1520/GTJ103596>, 2012.
- 669 [50] Wen, Y., Kasielke, T., Li, H., Zepp, H., and Zhang, B.: A case-study on history and rates of gully erosion in
670 Northeast China, Land Degrad. Dev., 32, 4254-4266, <https://doi.org/10.1002/ldr.4031>, 2021.
- 671 [51] Wen, Y., Liu, B., Jiang, H., Li, T., Zhang, B., and Wu, W.: Initial soil moisture prewinter affects the freeze-
672 thaw profile dynamics of a Mollisol in Northeast China, Catena, 234,
673 <https://doi.org/10.1016/j.catena.2023.107648>, 2024.
- 674 [52] Wang, F., Tian, P., Guo, W., Chen, L., Gong, Y., and Ping, Y.: Effects of rainfall patterns, vegetation cover
675 types and antecedent soil moisture on run-off and soil loss of typical Luvisol in southern China, Earth Surf
676 Process Landf., 49, 2998-3012, <https://doi.org/10.1002/esp.5871>, 2024.
- 677 [53] Xu, X., Zheng, F., Wilson, G. V., and Wu, M.: Upslope inflow, hillslope gradient and rainfall intensity impacts
678 on ephemeral gully erosion, Land Degrad. Dev., 28, 2623-2635, <https://doi.org/10.1002/ldr.2825>, 2017.
- 679 [54] Xu, X., Zheng, F., Wilson, G. V., He, C., Lu, J., and Bian, F.: Comparison of runoff and soil loss in different
680 tillage systems in the Mollisol region of Northeast China, Soil Tillage Res., 177, 1-11,
681 <https://doi.org/10.1016/j.still.2017.10.005>, 2018.
- 682 [55] Xu, X., Ma, Y., Yang, W., Zhang, H., Tarolli, P., Jiang, Y., and Yan, Q.: Qualifying mass failures on loess gully
683 sidewalls using laboratory experimentation, Catena, 187, <https://doi.org/10.1016/j.catena.2019.104252>, 2020.
- 684 [56] Yang, J., Zhang, S., Chang, L., Li, F., Li, T. Q., and Gao, Y.: Gully erosion regionalization of black soil area
685 in northeastern China, Chin. Geogr. Sci., 27, 78-87, <https://doi.org/10.1007/s11769-017-0848-z>, 2017.
- 686 [57] Zare, M., Soufi, M., Nejabat, M., and Pourghasemi, H. R.: The topographic threshold of gully erosion and

- 687 contributing factors, *Nat. Hazard*, 112, 2013-2035, <https://doi.org/10.1007/s11069-022-05254-6>, 2022.
- 688 [58] Zhang, S., Jiang, L., Liu, X., Zhang, X., Fu, S., and Dai, L.: Soil nutrient variance by slope position in a
689 Mollisol farmland area of Northeast China, *Chin. Geogr. Sci.*, 26, 508-517, [https://doi.org/10.1007/s11769-](https://doi.org/10.1007/s11769-015-0737-2)
690 015-0737-2, 2016.
- 691 [59] Zhang, S., Wang, X., Xiao, Z., Qu, F., Wang, X., Li, Y., Aurangzeib, M., Zhang, X., and Liu, X.: Quantitative
692 studies of gully slope erosion and soil physiochemical properties during freeze-thaw cycling in a Mollisol
693 region, *Sci. Total Environ.*, 707, <https://doi.org/10.1016/j.scitotenv.2019.136191>, 2020.
- 694 [60] Zhang, S., Han, X., Cruse, R., Zhang, X., Hu, W., Yan, Y., and Guo, M.: Morphological characteristics and
695 influencing factors of permanent gully and its contribution to regional soil loss based on a field investigation
696 of 393 km² in Mollisols region of northeast China, *Catena*, 217, <https://doi.org/10.1016/j.catena.2022.106467>,
697 2022.
- 698 [61] Zhou, P., Guo, M., Zhang, X., Zhang, S., Qi, J., Chen, Z., Wang, L., and Xu, J.: Quantifying the effect of
699 freeze-thaw on the soil erodibility of gully heads of typical gullies in the Mollisols region of Northeast China,
700 *Catena*, 228, <https://doi.org/10.1016/j.catena.2023.107180>, 2023.